Circulation Reports
Circ Rep 2024; 6: 564–572
doi:10.1253/circrep.CR-24-0086

ORIGINAL ARTICLE
Imaging

Machine Learning for Evaluating Vulnerable Plaque on Coronary Computed Tomography Using Spectral Imaging

Junji Mochizuki, MSc, RT; Yoshiki Hata, MD, PhD; Takeshi Nakaura, MD, PhD; Katsushi Hashimoto, MD, PhD; Hiroyuki Uetani, MD, PhD; Yasunori Nagayama, MD, PhD; Masafumi Kidoh, MD, PhD; Yoshinori Funama, PhD; Toshinori Hirai, MD, PhD

Background: This study aimed to determine whether spectral imaging with dual-energy computed tomography (CT) can improve diagnostic performance for coronary plaque characterization.

Methods and Results: We conducted a retrospective analysis of 30 patients with coronary plaques, using coronary CT angiography (dual-layer CT) and intravascular ultrasound (IVUS) studies. Based on IVUS findings, patients were diagnosed with either vulnerable or stable plaques. We computed 7 histogram parameters for plaque CT numbers in 120 kVp images and virtual monochromatic images ranging from 40 to 140 keV at 5-keV intervals. A predictive model was developed using histogram data of optimal energy, plaque volume or stenosis, and a combination of both. The model's performance was evaluated by calculating the area under the receiver operating characteristic curve (AUC) using 5-fold cross-validation. Peak diagnostic performances for each histogram parameter were observed at various energy levels (40–110 keV) in the univariate logistic regression model. The histogram model demonstrated optimal diagnostic performance at 65 keV, with an AUC of 0.81. The combined model, incorporating histogram data and plaque volume, achieved an AUC of 0.85, which was similar to the performance of qualitative CT characteristics (AUC=0.88; P=0.70).

Conclusions: Spectral imaging with dual-energy CT can enhance the diagnostic performance of machine learning using CT histograms for coronary plaque characterization.

Key Words: Coronary plaque characterization; Dual-energy CT; Histogram parameters; Machine learning; Spectral imaging

Identifying vulnerable plaque in coronary arteries, a contributory factor for myocardial infarction, is crucial. Conventionally, coronary plaques can only be evaluated using invasive methodologies such as intravascular ultrasound (IVUS). Cardiac computed tomography (CT) angiography has emerged as a promising non-invasive technique for detecting vulnerable plaques prior to a subsequent coronary event.[1–7] Characteristics of vulnerable plaque include low attenuation areas, positive remodeling, spotty calcification, ring-like sign, and plaque ulceration with intraplaque contrast penetration.[8–11] The mean CT score is useful for characterizing coronary plaques. Motoyama et al. classified non-calcified plaques into lipid-rich plaque (cut-off <30 HU) and fibrous plaque (30–150 HU).[8] However, overlapping lipid and fibrous plaque attenuation posed a limitation.[10,12–14]

The efficacy of CT analysis in plaque diagnosis has been reported to be superior with dual-energy techniques (DECT).[15–20] Ohta et al. demonstrated that the virtual monochromatic image (VMI) obtained from DECT optimizes image quality at distinct energy levels for various components of coronary plaque.[21] It has been suggested that comparing CT numbers at low and high energy settings may facilitate the differential diagnosis of lipid-rich plaque and other plaque types.[19] Furthermore, a histogram analysis using machine learning has been reported to surpass conventional cut-off methods in coronary plaque diagnosis using plaque CT numbers in cardiac CT images.[22,23] Although these 2 techniques may hold significant diagnostic potential, no current reports exist on their combined usage, and the optimal X-ray energy for plaque evaluation remains undetermined.

Received July 29, 2024; revised manuscript received September 20, 2024; accepted October 15, 2024; J-STAGE Advance Publication released online November 13, 2024 Time for primary review: 13 days
Minamino Cardiovascular Hospital, Tokyo (J.M., Y.H., K.H.); Department of Diagnostic Radiology, Graduate School of Medical Sciences, Kumamoto University, Kumamoto (T.N., H.U., Y.N., M.K., T.H.); and Department of Medical Physics, Faculty of Life Sciences, Kumamoto University, Kumamoto (Y.F.), Japan
Mailing address: Takeshi Nakaura, MD, PhD, Department of Diagnostic Radiology, Graduate School of Medical Sciences, Kumamoto University, 1-1-1 Honjo, Chuo-ku, Kumamoto, Kumamoto 860-8556, Japan. email: kff00712@nifty.com
All rights are reserved to the Japanese Circulation Society. For permissions, please email: cr@j-circ.or.jp
ISSN-2434-0790

Our hypothesis posits that the precision of plaque characterization can be enhanced by machine learning 3-dimensional plaque histogram evaluation using VMIs.

The aim of this study was to assess the diagnostic performance of machine learning on variable plaques based on 3-dimensional histograms of VMI obtained from spectral CT and to investigate the optimal energy of VMI.

Methods

This retrospective study received institutional review board approval; written informed consent was waived. The study included patients who underwent cardiac CT scans in our hospital from January 2017 to March 2019 and had clinical records of severe stenosis. All procedures performed in this study were in accordance with the ethical standards of the institutional research committee and with the 1964 Declaration of Helsinki and its later amendments or comparable ethical standards.

Cardiac CT Image Acquisition

All patients were scanned with a dual-layer spectral detector CT scanner (iQon Spectral CT; Philips Healthcare). Patients received sublingual nitroglycerin. Standard coronary CT angiography was performed using a 13-s intravenous infusion of 18.0 mgI/mL/s (Iopamiron 370; Bayer HealthCare). Contrast medium delivery was followed by flushing with 30 mL of physiological saline at the same injection rate. The acquisition parameters for cardiac CT imaging were as follows (**Table 1**): detector collimation 64×0.625 mm; tube rotation time 270 ms; tube voltage 120 kVp; tube current 436.1±103 mA (range 290–611 mA); and volume CT dose index 57.9±18.0 mGy (range 33.0–93.8 mGy).

Table 1. Scanning Parameters and Contrast Medium Infusion Protocol

Scanning parameter	
Tube voltage (kVp)	120
Tube current (effective mAs)	Auto mA
Helical pitch	0.16
Detector collimation (mm)	64×0.625
Rotation time (s)	0.27
Detector collimation (mm)	64×0.625
Rotation time (s)	0.27
Iodine dose (mgI/kg)	240
Bolus tracking trigger (HU)	110
Scan delay (s)	6
Injection duration (s)	13

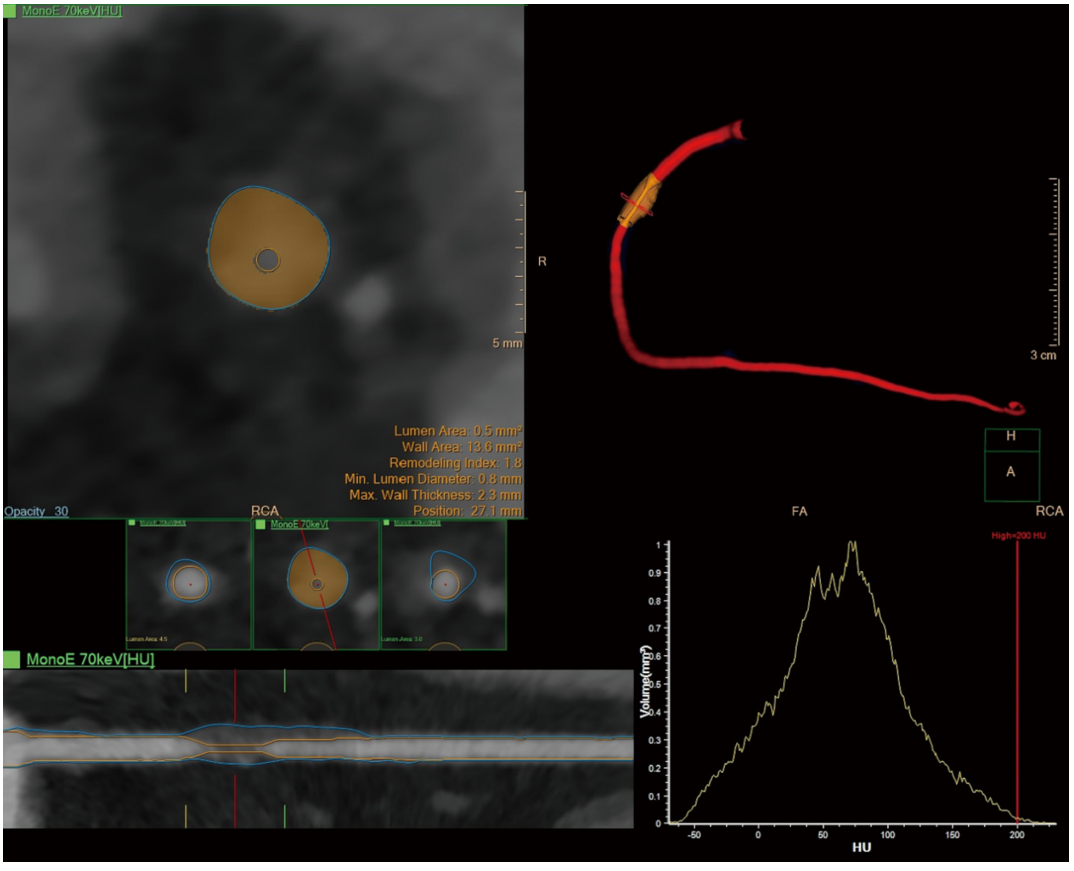

Figure 1. Plaque analysis. Three-dimensional histogram analysis created using specialized software. Plaque identification and voxel quantification were conducted semi-automatically, and the resultant histogram data was used for analysis.

CT Image Reconstruction

Spectral-based image data were post-processed on a workstation (Spectral Diagnostic Suite; Philips Healthcare) to generate VMIs at 21 distinct energy levels (40–140 keV), with a spectral level of 3 (manufacturer's recommendation). Conventional CT images reconstructed with IR (iDose level 3; Philips Healthcare) were used as controls. The spectral level and iDose level represent successive approximation reconstructions, and level 3 was chosen based on the manufacturer's recommendation. The slice thickness/increment of all CT images was 0.8 mm/0.4 mm.

IVUS

The subjects of this study will undergo coronary angiography and FFR to evaluate ischemia. If the FFR is ≤0.80, the diagnosis will be lesion-specific ischemia, and IVUS will then be performed. Target lesions were imaged using IVUS following intracoronary injection of nitroglycerin (1.0 mg). IVUS images were acquired using a 40-MHz IVUS imaging catheter (OptiCross, Boston Scientific Corporation) and an IVUS system (iLAB; Boston Scientific Corporation). Digital copies of the obtained images were preserved for subsequent offline analysis. IVUS analysis was conducted every 1.0 mm, independent of the cardiac cycle, using established software (QIvus 2.1; Medis Medical Imaging Systems, Leiden). The criteria derived from a clinical expert consensus document on guidelines for measurement and evaluation of IVUS from the Japanese Association of Cardiovascular Intervention and Therapeutics were used for grayscale IVUS analysis.[24] Specifically, vulnerable plaques were characterized by having at least 2 of the following known attributes of rupture-prone plaques as observed by IVUS: attenuated plaques, positive remodeling, and spotty calcification and a minimal lumen area of <4.0 mm^2 by IVUS; or a plaque burden of >70% by IVUS.[25,26] The analysis was performed by 2 cardiologists with over 20 years of experience.

Analysis of Coronary CTA Data and Plaque Quantification

Image analysis was conducted by a radiology technologist with 17 years of experience using dedicated cardiac analysis software (Cardiac Viewer and Comprehensive Cardiac Analysis, intelliSpace Portal, Philips Healthcare) and a plaque analysis application for the assessment of non-calcified coronary plaque volume and various characteristics (**Figure 1**). Semi-automatic lesion identification, characterization, and quantification were performed using a plaque volume analysis program integrated with the dedicated cardiac analysis software.[27] The remodeling index (RI) is defined as the ratio of the maximum vessel area to a normal reference vessel area, and plaques are classified as having significant positive remodeling when the RI is >1.1.[28] The presence of the napkin-ring sign, characterized by a low-attenuating plaque core surrounded by an area of higher attenuation, was evaluated.[29] Spotty calcifications were visually examined as calcifications covering <90° of the lesion circumference and measuring <3 mm in length.[30] Low attenuation plaques were defined as CT number >30 HU.[31] Societal guidelines using the coronary artery disease reporting and data system (CAD-RADS™) were used to determine the degree of stenosis: (1) none (0%), or minimal (1–24% stenosis); (2) mild (25–49% stenosis); (3) moderate (50–69% stenosis); (4) severe (70–99% stenosis); and (5) total occlusion (100%).[32] Several sequential image processing steps were undertaken, including automatic model-based whole-heart segmentation, automatic extraction of the coronary tree and centerline, automatic luminal and vessel wall contouring, and semi-automatic plaque examination. Plaque volumes were measured and 3-dimensional histograms of plaque extracts at each VMI and 120 kVp were generated. We also calculated 7 histogram parameters (minimum and mean value, standard deviation, maximum value, skewness, kurtosis, and entropy) of the plaque CT number of 120 kVp images and VMI using Python (version 3.8.5; https://www.python.org).

Training of Machine Learning Models

Due to the limited number of cases, partitioning the training and test groups was infeasible. Consequently, the cross-validation function of scikit-learn was used, which automatically divided the population into 5-fold cross-validation for training and learning purposes. To assess the discriminative ability and optimal energy of each histogram parameter individually for distinguishing between vulnerable and stable plaques, univariate logistic regression was used to train all histogram parameters at all VMIs and 120 kVp, followed by an evaluation. Subsequently, to evaluate the discriminative ability and optimal energy of ML using all histogram parameters of VMI, Random Forest was trained and assessed for all VMIs and 120 kVp. The optimal parameters of Random Forest were determined through the grid search technique.

Furthermore, after determining the optimal energy, we developed a combined model incorporating the histogram parameters at the optimal energy level along with other significant factors. These factors included coronary stenosis and plaque volume measurements that showed statistically significant differences between vulnerable and stable plaques. This combined model aimed to enhance the overall predictive performance by integrating multiple relevant features.

To evaluate the performance of these models, we established a reference standard based on qualitative CT characteristics. This standard was derived from the sum of scores for the presence or absence of previously mentioned features: low attenuation areas, positive remodeling, spotty calcification, and the ring-like sign. This model served as a benchmark to compare the performance of our developed models against the traditional qualitative approach, allowing us to assess potential improvements in plaque vulnerability assessment.

Statistical Analysis

We compared patient's characteristics and plaque characteristics of vulnerable and stable plaques using the Mann-Whitney U test. The area under the curve (AUC) of our receiver operating characteristic (ROC) analysis of machine learning and conventional CT number-based classifiers was calculated. We compared the diagnostic performance of the machine learning and conventional CT number-based AUCs using the DeLong test. A P value <0.05 was deemed a statistically significant difference. We also calculated the importance of all features. All statistical analyses were performed using Python (version 3.8.5).

Results

Study Population

During the study period, cardiac CT was conducted in 5,679 patients with clinically suspected or confirmed coro-

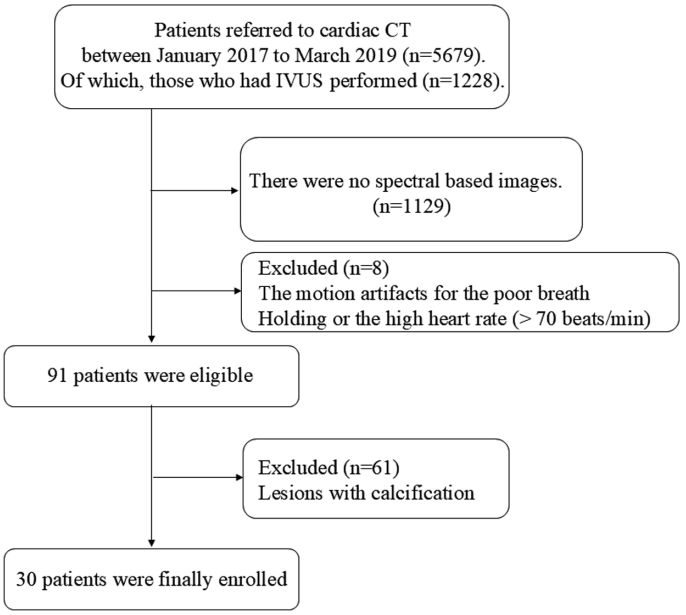

Figure 2. Flowchart of patient inclusion criteria. CT, computed tomography; IVUS, intravascular ultrasound.

Table 2. Patient Demographics

	All (n=30)	Vulnerable plaques (n=17)	Stable plaques (n=13)	P value
Age (years)	68.0±10.6	68.8±11.4	66.7±9.2	0.59
Male	24 (80)	13 (76)	11 (85)	0.58
Hypertension	11 (37)	5 (29)	11 (37)	0.35
Hyperlipidaemia	23 (77)	14 (82)	3 (23)	0.40
Diabetes	7 (23)	4 (24)	7 (23)	0.98
Smoking	11 (37)	7 (41)	4 (31)	0.56

Data are presented as n (%), or mean±SD.

Table 3. Comparison of Computed Tomography Characteristics in Vulnerable and Stable Coronary Plaques

	All (n=30)	Vulnerable plaques (n=17)	Sable plaques (n=13)	P value
Stenosis ≥70%	30 (100)	17 (100)	13 (100)	1.00
Plaque volume (mm^3)	26.5±10.0	32.1±17.2	21.2±12.0	0.08
Positive remodeling (RI ≥1.1)	13 (43)	11 (65)	2 (15)	<0.01
Napkin-ring sign	6 (20)	5 (29)	1 (8)	0.13
Spotty calcification	13 (43)	10 (59)	3 (23)	0.05
Low attenuation plaque (≤30 HU)	25 (83)	16 (94)	9 (69)	0.07

Data are presented as n (%), or mean±SD. RI, remodeling index.

nary artery disease, following the American College of Cardiology guidelines.[33] Of these, 4,451 had no IVUS, 1,129 had no dual-energy data, and 8 were excluded due to motion artifacts and poor image quality. Of the 91 remaining patients, 61 with severe calcified lesions were excluded, and the remaining 30 patients were enrolled in this study. The study group included 25 men and 5 women with a mean age of 68 years (range 48–86 years), a mean body weight of 66.1 kg (range 48.2–99.6 kg), and a mean eGFR of 60.1 mg/dL (range 51.5–69.6; **Figure 2**). All subjects were diagnosed with chronic coronary artery disease. The disease site was the right coronary artery in 6 patients, left anterior descending artery in 22 patients, and left circumflex artery in 2 patients. Of the total 30 lesions in the study, IVUS analysis classified 17 lesions as vulnerable plaques and 13 lesions as stable plaques. In the comparison between vulnerable and stable plaques, there were no significant differences in the prevalence of hypertension, hyperlipidemia, diabetes, or smoking status (**Table 2**).

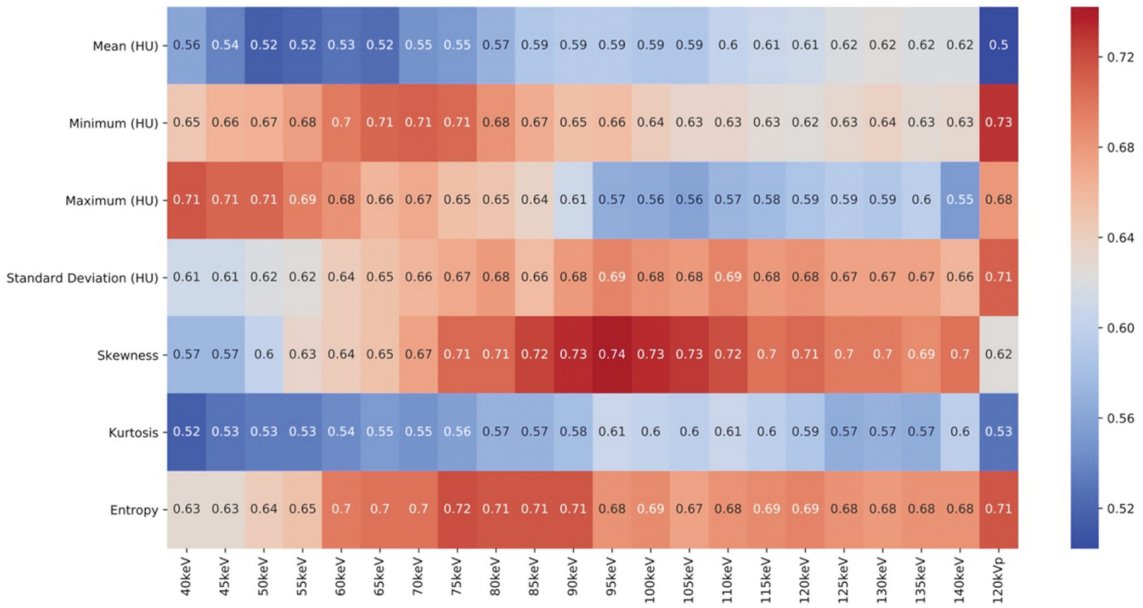

Figure 3. Area under the curves of each histogram parameter. Area under the curve for each energy level (40–140 keV) in the univariate logistic regression model; however, the optimal virtual monochromatic image energy varied for each histogram parameter.

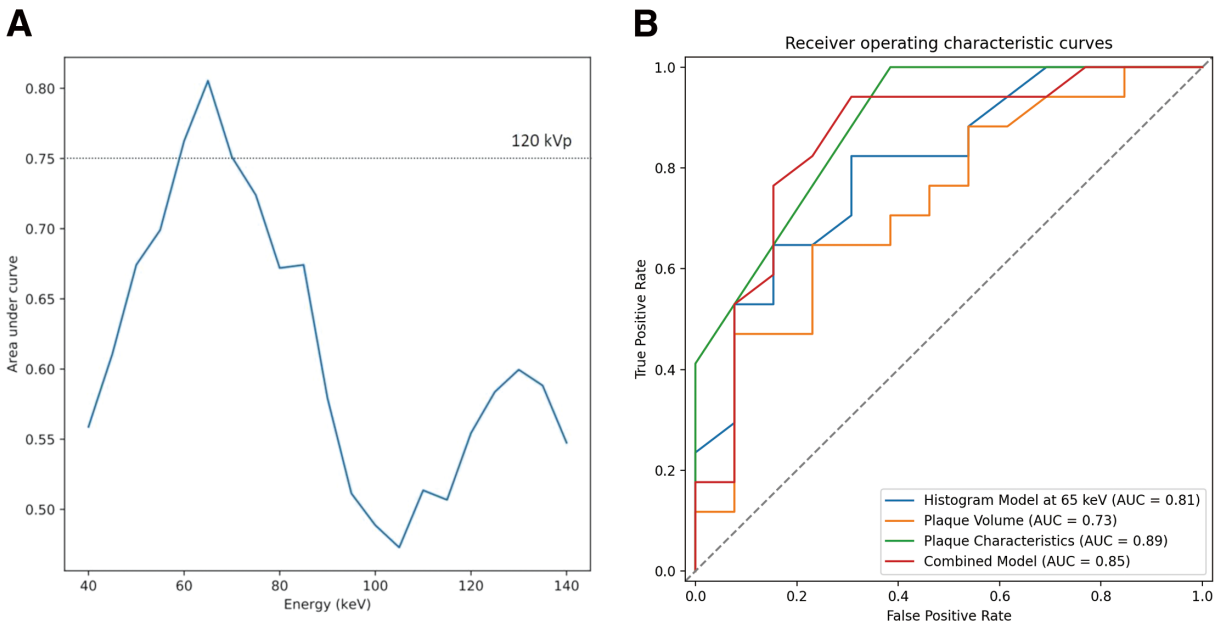

Figure 4. Area under the curves (AUC) of various prediction models. AUC of Random Forest at different energy levels (**A**), and the receiver operating characteristic (ROC) curves (**B**) of the histogram model at 65 keV (AUC=0.81), plaque volume (AUC=0.73), plaque characteristics (AUC=0.89), and the combined model (AUC=0.85).

Qualitative Assessment of the CT Characteristics

All plaques in both groups exhibited stenosis ≥70%. While plaque volume tended to be larger in vulnerable plaques compared with stable plaques (32.1±17.2 mm^3 vs. 21.2±12.0 mm^3; P=0.08), this difference did not reach statistical significance. Positive remodeling (RI ≥1.1) was significantly more prevalent in vulnerable plaques compared with stable plaques (65% vs. 15%; P<0.01). The napkin-ring sign was observed more frequently in vulnerable plaques, but this difference was not statistically significant

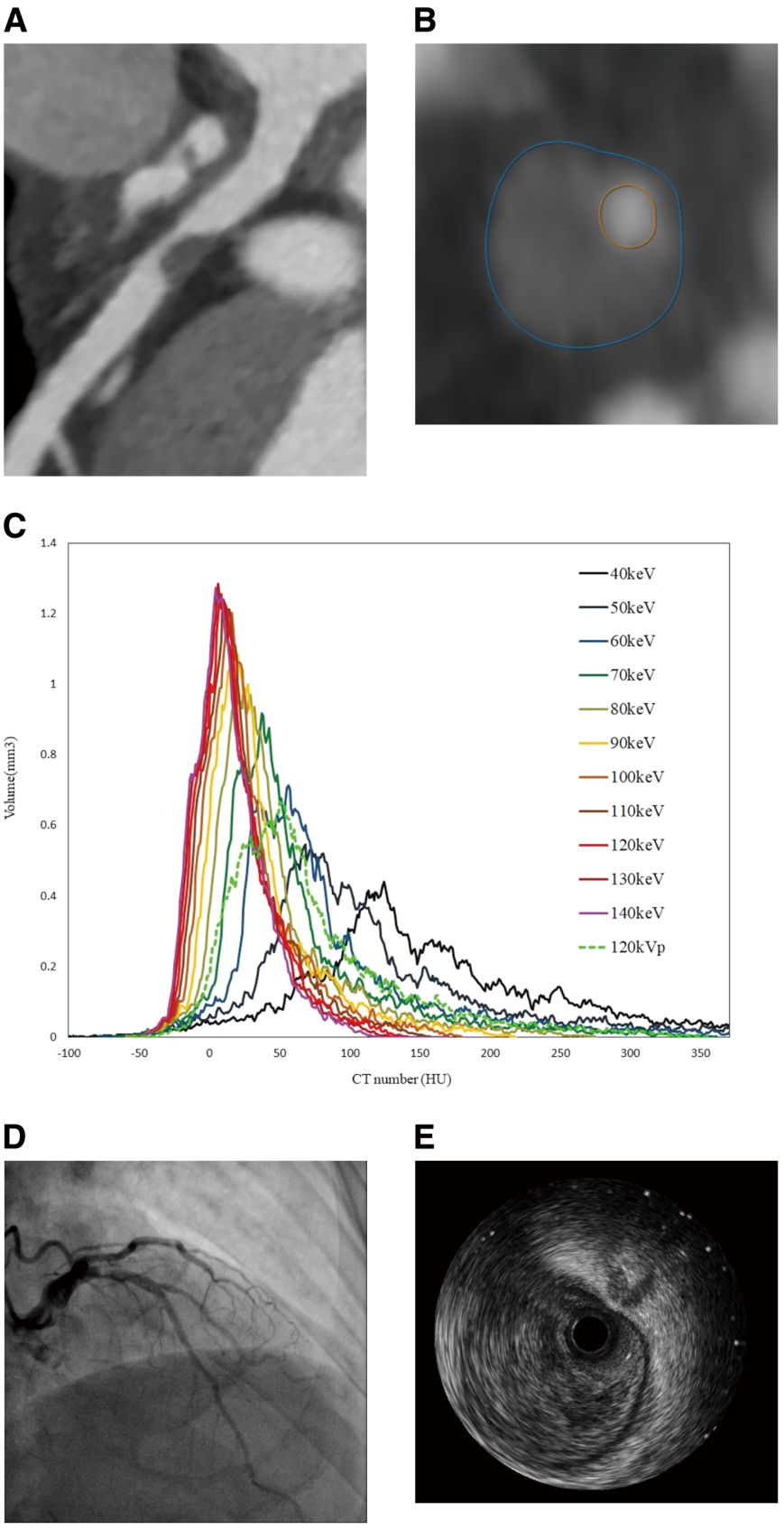

Figure 5. Representative case. Cardiac computed tomography (CT) curved multiplanar image (**A**) and short-axis image (**B**) showed stenosis in the left anterior descending artery #6. Plaque histograms (**C**) at 120 kVp and virtual monochromatic image at different energies showed that the histogram shape changed with energy. Angiography (**D**) and intravascular ultrasound (**E**) showed a vulnerable plaque. In this case, the spectral imaging analysis indicated that the plaques were unstable. As a result, distal protection was used to prevent embolization; after percutaneous coronary intervention, there was a transient reduction in blood flow that quickly recovered.

(29% vs. 8%; P=0.13). Spotty calcification showed a trend towards higher prevalence in vulnerable plaques (59% vs. 23%; P=0.05). Similarly, low attenuation plaque (≤30 HU) was more common in vulnerable plaques, although this difference did not reach statistical significance (94% vs. 69%; P=0.07; **Table 3**).

Model Performance Comparison

Using the univariate logistic regression model, the peak diagnostic performance of each histogram parameter was observed at different energy levels (40–140 keV; **Figure 3**). The AUCs were as follows: mean (0.62; 125–140 keV); minimum (0.73; 120 kVp); maximum (0.71; 40 keV, 45 keV, and 50 keV); standard deviation (0.71; 120 kVp); skewness (0.74; 95 keV); kurtosis (0.61; 95 keV, and 110 keV); and entropy (0.72; 75 keV; **Figure 3**).

Using the Random Forest model combining all features, peak diagnostic performance was observed at 65 keV (AUC=0.81; **Figure 4A**). The AUC of the 65 keV Random Forest model (AUC 0.81) was significantly higher than that of the 120 kVp Random Forest model (AUC 0.72) and the mean CT number (AUC 0.50) using 120 kVp images (P<0.05). Since there was no significant difference in stenosis, a prediction model was created using only plaque volume, resulting in an AUC of 0.73. The combined model, incorporating histogram data and plaque volume, achieved an AUC of 0.85, which was similar to the performance of qualitative CT characteristics (AUC=0.88; P=0.70; **Figure 4B**). Representative cases are shown in **Figure 5**.

Discussion

The present study suggests that the diagnostic performance of machine learning for coronary vulnerable plaques, utilizing VMI and 3-dimensional histogram parameters, is significantly superior with VMI 65 keV compared with 120 kVp images.

Previous reports have suggested that DECT is a valuable tool for diagnosing coronary plaques. An ex vivo study of 20 human arteries showed that CT number-based characterization of non-calcified plaques using DECT demonstrated selective improvement over conventional CT.[19] Furthermore, spectral coronary CTA with low-energy (40–70 keV) post-processing has been reported to enhance the CNR of coronary plaque components.[20] At diagnostic energies, Compton scatter and photoelectric absorption, both dependent on the material's atomic number, are responsible for X-ray attenuation. These interactions vary with the energy provided. Using various X-ray energies, Barreto et al. observed a substantial variation in the attenuation of fibrous plaque but not the lipid-rich necrotic core.[15] The precise cause of this phenomenon is challenging to explain, but previous reports have shown that vulnerable plaques are lipid-rich and influenced by blood flow.[34] Consequently, it is possible that lower energy did not reveal a difference from stable plaques due to both a reduction in fat absorption and an increase in the contrast effect. If the lipid-rich plaque was minuscule, additional tissue types may have been present in the CT region sample.

In the univariate logistic regression analysis, the optimal VMI energy differed for each histogram parameter; no CT number difference was observed, but the diagnostic performance was superior at lower energies. The minimum CT number demonstrated reasonable results at moderate energies (65–75 keV), while the maximum CT number performed better at lower energies (40–50 keV). This phenomenon may be attributable to the fact that stable plaques have a high fibrous component, causing CT numbers to increase with lower energy and potentially creating the observed difference. The skewness and entropy AUCs exhibited a favorable trend in the intermediate energy range. This outcome may be influenced by the image quality of the VMI, with extremely low energy VMIs increasing noise and possibly not displaying an accurate CT number.

The study findings indicate that the diagnostic efficacy of the histogram analysis approach with machine learning is sensitive to the energy parameters used in dual-energy CT. Histogram analysis can scrutinize the distribution of pixel intensities within an image to appraise fine calcifications and lipids in vulnerable plaques. Given these lesions are minute and characterized by scarce differences in CT values, a highly accurate approach is required to detect them. The 65 keV images, identified as the most suitable energy VMI in this investigation, exhibited superiority over traditional 120 kVp images. In addition to superior spatial and contrast resolution balance, the utilization of VMI benefits, such as beam hardening correction, were believed to have contributed to the positive outcomes obtained.

Another significant finding of this study is that the diagnostic performance of the combined model, which incorporates histogram data at optimal energy and plaque volume (AUC=0.85), is comparable with that of qualitative plaque analysis (AUC=0.88). This observation has important clinical implications. While the model's value may be limited in centers with extensive experience in cardiac CT evaluation, it offers substantial benefits in other settings. Notably, it enables individuals without specialized knowledge to achieve diagnostic accuracy like that of expert centers by simply measuring coronary plaque volume and analyzing histograms. This democratization of diagnostic capability could significantly impact clinical practice, particularly in areas with limited access to specialized cardiac imaging expertise. Furthermore, this approach lays the groundwork for potential future developments, such as automated systems that could alert referring physicians or radiologists to the presence of vulnerable plaques. Such advancements could enhance early detection and risk stratification in coronary artery disease, potentially improving patient outcomes through timely interventions.

Study Limitations

The limitations of this study should be acknowledged. First, this investigation was conducted as a small-scale, single-center study following a single protocol. The limited sample size prevented us from performing multiple comparisons across the various energy levels examined in this study. Our methodological approach relied on cross-validation techniques without establishing a separate test group, which underscores the need for larger-scale studies with dedicated test sets to fully assess the model's generalizability. Second, although the study used IVUS to evaluate the results, there was a selection bias in the participating centers. Last, the small sample size precluded further analyses, such as subgroup comparisons based on patient data or multiple comparisons across different parameters. These limitations highlight the need for more comprehensive, multi-center studies with larger sample sizes to validate and extend our findings.

Conclusions

Spectral imaging with dual-energy CT can enhance the diagnostic performance of machine learning using CT histograms for coronary plaque characterization.

Acknowledgment

We thank the team at the Minamino Cardiovascular Hospital for their help with performing the study.

Sources of Funding

This research did not receive any specific grant from funding agencies in the public, commercial, or not-for-profit sectors.

Disclosures

T.N. has received research support from Nemoto Kyorindo Co., Ltd. T.H. has received research support from Canon Medical Systems. The department of diagnostic imaging analysis, to which M.K. belongs, is an endowed chair supported by Philips Healthcare. The Nemoto Kyorindo Co., Ltd, Philips Healthcare and Canon Medical Systems had no control over the interpretation, writing, or publication of this work.

IRB Information

This retrospective study received institutional review board approval (MJ-023, 'Coronary plaque assessment by Spectral CT'). Written informed consent was waived.

Data Availability

The datasets generated or analyzed during the study are available from the corresponding author on reasonable request.

References

1. Goldstein JA, Dixon S, Safian RD, Hanzel G, Grines CL, Raff GL. Computed tomographic angiographic morphology of invasively proven complex coronary plaques. *JACC Cardiovasc Imaging* 2008; **1:** 249–251, doi:10.1016/j.jcmg.2008.01.010.
2. Hecht HS, Achenbach S, Kondo T, Narula J. High-risk plaque features on coronary CT angiography. *JACC Cardiovasc Imaging* 2015; **8:** 1336–1339, doi:10.1016/j.jcmg.2014.11.018.
3. Matsumoto H, Watanabe S, Kyo E, Tsuji T, Ando Y, Otaki Y, et al. Standardized volumetric plaque quantification and characterization from coronary CT angiography: A head-to-head comparison with invasive intravascular ultrasound. *Eur Radiol* 2019; **29:** 6129–6139, doi:10.1007/s00330-019-06219-3.
4. Nakazato R, Shalev A, Doh JH, Koo BK, Gransar H, Gomez MJ, et al. Aggregate plaque volume by coronary computed tomography angiography is superior and incremental to luminal narrowing for diagnosis of ischemic lesions of intermediate stenosis severity. *J Am Coll Cardiol* 2013; **62:** 460–467, doi:10.1016/j.jacc.2013.04.062.
5. Obaid DR, Calvert PA, Brown A, Gopalan D, West NEJ, Rudd JHF, et al. Coronary CT angiography features of ruptured and high-risk atherosclerotic plaques: Correlation with intra-vascular ultrasound. *J Cardiovasc Comput Tomogr* 2017; **11:** 455–461, doi:10.1016/j.jcct.2017.09.001.
6. Opolski MP, Kepka C, Witkowski A. CT evaluation of vulnerable plaque: Noninvasive fortune-telling? *Int J Cardiovasc Imaging* 2012; **28:** 1613–1615, doi:10.1007/s10554-011-9875-5.
7. Kawai H, Motoyama S, Sarai M, Ito H, Takahashi H, Harigaya H, et al. Adding coronary computed tomography angiography to invasive coronary angiography improves prediction of cardiac events. *Circ J* 2014; **78:** 2735–2740, doi:10.1253/circj.CJ-14-0743.
8. Motoyama S, Sarai M, Harigaya H, Anno H, Inoue K, Hara T, et al. Computed tomographic angiography characteristics of atherosclerotic plaques subsequently resulting in acute coronary syndrome. *J Am Coll Radiol* 2009; **54:** 49–57, doi:10.1016/j.jacc.2009.02.068.
9. Munnur RK, Cameron JD, Ko BS, Meredith IT, Wong DTL. Cardiac CT: Atherosclerosis to acute coronary syndrome. *Cardiovasc Diagn Ther* 2014; **4:** 430–448, doi:10.3978/j.issn.2223-3652.2014.11.03.
10. Saremi F, Achenbach S. Coronary plaque characterization using CT. *Am J Roentgenol* 2015; **204:** W249–W260, doi:10.2214/AJR.14.13760.
11. Sato A, Aonuma K. Role of cardiac multidetector computed tomography beyond coronary angiography. *Circ J* 2015; **79:** 712–720, doi:10.1253/circj.CJ-15-0102.
12. Higashi M. Noninvasive assessment of coronary plaque using multidetector row computed tomography: Does MDCT accurately estimate plaque vulnerability? (Con) *Circ J* 2011; **75:** 1522–1528, doi:10.1253/circj.CJ-11-0313.
13. Leber AW, Becker A, Knez A, von Ziegler F, Sirol M, Nikolaou K, et al. Accuracy of 64-slice computed tomography to classify and quantify plaque volumes in the proximal coronary system. *J Am Coll Cardiol* 2006; **47:** 672–677, doi:10.1016/j.jacc.2005.10.058.
14. Liu H, Wingert A, Wang J, Zhang J, Wang X, Sun J, et al. Extraction of coronary atherosclerotic plaques from computed tomography imaging: A review of recent methods. *Front Cardiovasc Med* 2021; **8:** 597568, doi:10.3389/fcvm.2021.597568.
15. Barreto M, Schoenhagen P, Nair A, Amatangelo S, Milite M, Obuchowski NA, et al. Potential of dual-energy computed tomography to characterize atherosclerotic plaque: Ex vivo assessment of human coronary arteries in comparison to histology. *J Cardiovasc Comput Tomogr* 2008; **2:** 234–242, doi:10.1016/j.jcct.2008.05.146.
16. Danad I, Fayad ZA, Willemink MJ, Min JK. New applications of cardiac computed tomography. *JACC Cardiovasc Imaging* 2015; **8:** 710–723, doi:10.1016/j.jcmg.2015.03.005.
17. Mandal SR, Bharati A, Haghighi RR, Arava S, Ray R, Jagia P, et al. Non-invasive characterization of coronary artery atherosclerotic plaque using dual energy CT: Explanation in ex-vivo samples. *Phys Med* 2018; **45:** 52–58, doi:10.1016/j.ejmp.2017.12.006.
18. Matsumoto K, Jinzaki M, Tanami Y, Ueno A, Yamada M, Kuribayashi S. Virtual monochromatic spectral imaging with fast kilovoltage switching: Improved image quality as compared with that obtained with conventional 120-kVp CT. *Radiology* 2011; **259:** 257–262, doi:10.1148/radiol.11100978.
19. Obaid DR, Calvert PA, Gopalan D, Parker RA, West NEJ, Goddard M, et al. Dual-energy computed tomography imaging to determine atherosclerotic plaque composition: A prospective study with tissue validation. *J Cardiovasc Comput Tomogr* 2014; **8:** 230–237, doi:10.1016/j.jcct.2014.04.007.
20. Symons R, Choi Y, Cork TE, Ahlman MA, Mallek M, Bluemke DA, et al. Optimized energy of spectral coronary CT angiography for coronary plaque detection and quantification. *J Cardiovasc Comput Tomogr* 2018; **12:** 108–114, doi:10.1016/j.jcct.2018.01.006.
21. Ohta Y, Kitao S, Watanabe T, Kishimoto J, Yamamoto K, Ogawa T. Evaluation of image quality of coronary artery plaque with rapid kVp-switching dual-energy CT. *Clin Imaging* 2017; **43:** 42–49, doi:10.1016/j.clinimag.2017.01.014.
22. Kolossváry M, Karády J, Kikuchi Y, Ivanov A, Schlett CL, Lu MT, et al. Radiomics versus visual and histogram-based assessment to identify atheromatous lesions at coronary CT angiography: An ex vivo study. *Radiology* 2019; **293:** 89–96, doi:10.1148/radiol.2019190407.
23. Masuda T, Nakaura T, Funama Y, Okimoto T, Sato T, Higaki T, et al. Machine-learning integration of CT histogram analysis to evaluate the composition of atherosclerotic plaques: Validation with IB-IVUS. *J Cardiovasc Comput Tomogr* 2019; **13:** 163–169, doi:10.1016/j.jcct.2018.10.018.
24. Saito Y, Kobayashi Y, Fujii K, Sonoda S, Tsujita K, Hibi K, et al. Clinical expert consensus document on standards for measurements and assessment of intravascular ultrasound from the Japanese Association of Cardiovascular Intervention and Therapeutics. *Cardiovasc Interv Ther* 2020; **35:** 1–12, doi:10.1007/s12928-019-00625-6.
25. Nakao Y, Yoshida K, Inaba S, Tanabe Y, Kurata A, Uetani T, et al. Plaque characterization with computed tomography angiography based on a diluted-contrast injection protocol. *Intern Med* 2021; **60:** 3671–3678, doi:10.2169/internalmedicine.6683-20.
26. Park SJ, Ahn JM, Kang DY, Yun SC, Ahn YK, Kim WJ, et al. Preventive percutaneous coronary intervention versus optimal medical therapy alone for the treatment of vulnerable atherosclerotic coronary plaques (PREVENT): A multicentre, open-label, randomised controlled trial. *Lancet* 2024; **403:** 1753–1765, doi:10.1016/S0140-6736(24)00413-6.
27. Klass O, Kleinhans S, Walker MJ, Olszewski M, Feuerlein S, Juchems M, et al. Coronary plaque imaging with 256-slice multidetector computed tomography: Interobserver variability of

volumetric lesion parameters with semiautomatic plaque analysis software. *Int J Cardiovasc Imaging* 2010; **26:** 711–720, doi:10.1007/s10554-010-9614-3.
28. Giannopoulos AA, Benz DC, Gräni C, Buechel RR. Imaging the event-prone coronary artery plaque. *J Nucl Cardiol* 2019; **26:** 141–153, doi:10.1007/s12350-017-0982-0.
29. Maurovich-Horvat P, Schlett CL, Alkadhi H, Nakano M, Otsuka F, Stolzmann P, et al. The napkin-ring sign indicates advanced atherosclerotic lesions in coronary CT angiography. *JACC Cardiovasc Imaging* 2012; **5:** 1243–1252, doi:10.1016/j.jcmg.2012.03.019.
30. Park HB, Heo R, Ó Hartaigh B, Cho I, Gransar H, Nakazato R, et al. Atherosclerotic plaque characteristics by CT angiography identify coronary lesions that cause ischemia. *JACC Cardiovasc Imaging* 2015; **8:** 1–10, doi:10.1016/j.jcmg.2014.11.002.
31. Motoyama S, Kondo T, Sarai M, Sugiura A, Harigaya H, Sato T, et al. Multislice computed tomographic characteristics of coronary lesions in acute coronary syndromes. *J Am Coll Cardiol* 2007; **50:** 319–326, doi:10.1016/j.jacc.2007.03.044.
32. Cury RC, Abbara S, Achenbach S, Agatston A, Berman DS, Budoff MJ, et al. CAD-RADS™: Coronary artery disease – Reporting and data system. *J Am Coll Radiol* 2016; **13:** 1458–1466.e9, doi:10.1016/j.jacr.2016.04.024.
33. Doherty JU, Kort S, Mehran R, Schoenhagen P, Soman P, Dehmer GJ, et al. ACC/AATS/AHA/ASE/ASNC/HRS/SCAI/SCCT/SCMR/STS 2019 appropriate use criteria for multimodality imaging in the assessment of cardiac structure and function in nonvalvular heart disease: A report of the American College of Cardiology Appropriate Use Criteria Task Force, American Association for Thoracic Surgery, American Heart Association, American Society of Echocardiography, American Society of Nuclear Cardiology, Heart Rhythm Society, Society for Cardiovascular Angiography and Interventions, Society of Cardiovascular Computed Tomography, Society for Cardiovascular Magnetic Resonance, and the Society of Thoracic Surgeons. *J Am Coll Cardiol* 2019; **73:** 488–516, doi:10.1016/j.jacc.2018.10.038.
34. Kuroiwa Y, Uchida A, Yamashita A, Miyati T, Maekawa K, Gi T, et al. Coronary high-signal-intensity plaques on T1-weighted magnetic resonance imaging reflect intraplaque hemorrhage. *Cardiovasc Pathol* 2019; **40:** 24–31, doi:10.1016/j.carpath.2019.01.002.